Performance Analysis of Passive Magnetic Pointing Method for Implementation of Directional Antennas on CubeSats

Article *in* International Journal of Aeronautical and Space Sciences · March 2022

DOI: 10.1007/s42405-022-00448-5

CITATIONS
0

READS
1,146

1 author:

Christopher Anderson
United States Naval Academy
94 PUBLICATIONS **1,664** CITATIONS

SEE PROFILE

International Journal of Aeronautical and Space Sciences
https://doi.org/10.1007/s42405-022-00448-5

IJASS International Journal of Aeronautical and Space Sciences

ORIGINAL PAPER

Performance Analysis of Passive Magnetic Pointing Method for Implementation of Directional Antennas on CubeSats

Jin S. Kang[1] · Jeffery T. King[1] · Christopher R. Anderson[2] · Michael H. Sanders[1]

Received: 1 December 2021 / Revised: 1 February 2022 / Accepted: 4 February 2022

Abstract

As CubeSats have become hugely popular in the recent years, the demand on their capability has also increased. As the missions and functionalities become more complex, coupled with the popular VHF and UHF bands becoming less accessible, CubeSats have been getting pushed into using higher frequency bands. For more capable CubeSats such as NASA and military satellites, utilization of S- and X-band communication have become a common place. While S- and X-band communication provide much higher data rate for the mission, the power and attitude control demand has also increased. Meeting this increased cost and demand on resources may not be feasible for university-level projects as attitude control systems can often cost more than the rest of the CubeSat. This research revisits passive magnetic pointing as an option for providing antenna pointing capability for CubeSats, enabling S- and X-band communication without requiring an active attitude control system. CubeSats can make contact with ground stations located at higher latitude to establish data link with directional antennas. The analyses shows that a higher data throughput can be achieved using S- and X-band communication over the traditional 9600 bps link with the proposed setup, without requiring active attitude control or deployable solar panels. The study characterizes the expected communication link performance for a typical 3U CubeSat when implementing the proposed communication architecture using a S- or X-band patch antenna taking into consideration the expected pointing performance and power generation capability of a 3U CubeSat.

Keywords Spacecraft · Cubesat · Magnetic pointing · Attitude control · Communication

1 Introduction

With the recent growing popularity of CubeSat-class satellites for performing operational missions beyond the role of education, CubeSats' capabilities have also been dramatically improving [1]. Accordingly, the demand on data throughput performance of CubeSats has been steadily increasing. The previously-popular UHF and VHF frequency bands that CubeSats often use has become crowded. These two effects have driven CubeSats and small satellites to use higher and higher frequency bands such as S- and X-bands [2], which has been reflected in growing numbers of S- and X-band transmitters being commercially available for purchase. Government CubeSats, such as the ones developed at the United States Naval Academy (USNA), are also seeing an increased need to move into S-band communication and beyond. Many government CubeSats are even starting to adopt X-band for downlink communication.

While higher frequency RF communication provides a higher data rate, it also negatively affects the ability to close

Jeffery T. King, Christopher R. Anderson and Michael H. Sanders contributed equally to this work.

An earlier version of this paper was presented at APISAT 2021, Jeju, South Korea, in November 2021.

✉ Jin S. Kang
kang@usna.edu

Jeffery T. King
jking@usna.edu

Christopher R. Anderson
canderso@usna.edu

Michael H. Sanders
mhsander@usna.edu

[1] Aerospace Engineering Department, U.S. Naval Academy, 590 Holloway Rd. MS 11B, Annapolis, MD 21402, USA

[2] Electrical and Computer Engineering Department, U.S. Naval Academy, 597 McNair Rd., Annapolis, MD 21402, USA

Published online: 17 March 2022

the communications link. Transmission power and antenna gain has to be increased significantly to overcome the associated losses due to the higher carrier frequency. Since small satellites are often limited in power generation capability, a good balance between the increase in transmitted power and increasing antenna gain must be achieved. An increase in antenna gain means a highly directive antenna, which in turn requires the satellite antenna to be pointed towards the ground station antenna. Less complex satellites, typical of educational CubeSats, often employ simpler omni-directional antenna designs and do not have the ability to point their antennas. An addition of an attitude control system for antenna pointing purposes is often a big burden on the satellite in terms of volume, power consumption, increasing cost, and often is simply not feasible. For university-level CubeSat developers with small budgets, an off-the-shelf attitude control system cost can double or triple the overall satellite cost.

This constraint also applies to the Naval Academy's CubeSat projects. USNA develops and launches approximately one student-built CubeSat every year for education and training of the future space workforce. Accordingly, the satellite development projects need a standardized low-cost satellite bus, which in turn enables student education at a sustainable pace and cost. University satellites, such as USNA CubeSats, that operate with lower budget and faster development cycle require a viable satellite communication solution. VHF and UHF communications at a data rate of 9600 baud have been sufficient to meet the requirements of these student missions in the past. Adopting S- or X-band communication architectures poses significant step-up in satellite complexity because a directional high-gain antenna is required to maintain an acceptable link margin. An attitude control system that will allow the satellite antenna to be pointed towards the ground station can greatly increase the cost of the student CubeSat. To avoid this high cost alternative, a passive method for pointing the satellite is desired.

One solution to providing low-cost, passive attitude control is to use a permanent magnet in orienting the satellite, especially for CubeSats [3,4]. The permanent magnet on the satellite will create torque to align its axes to the local Earth's magnetic field line. Oscillation caused by this motion is usually damped by implementation of hysteresis material on the satellite. The method that is most often used is to utilize multiple permanent magnets aligned in the same direction, coupled with hysteresis material to provide rotational damping. While fine control or pointing cannot be accomplished using this method, it can still provide general attitude stability without requiring any power or control from the spacecraft. KySat-1 is an example of a satellite that employs passive magnetic attitude stabilization which included 24 small permanent magnets installed along its rails, along with HyMu80 sheet metal strips for magnetic damping [5,6]. On a slightly larger scale, UNISAT-4 also used the similar setup of permanent magnets and hysteresis rods combination for passive attitude stabilization [7]. Predicting the expected performance of magnetic hysteresis material is not trivial, but there have been many studies that have characterized the on-orbit magnetic damping properties of these hysteresis bars and strips through simulation and experiments [8–11]. While the permanent magnet coupled with magnetic damping can provide attitude stabilization, the method cannot be utilized for general directional pointing. When a satellite or a payload needs to face a certain direction, passive magnetic stabilization cannot provide that pointing capability because the satellite attitude will depend on the local direction of the magnetic field, which may or may not align with the desired direction of pointing. For this reason, small satellites utilizing passive magnetic pointing method depend on omni-directional antennas for communication with the ground.

Another passive attitude stabilization method that can provide nadir pointing is using a gravity gradient boom where the differential gravity acting on separated masses causes the satellite to align itself with the gravity vector. One major drawback of this method is that equal chance exists for either end of the satellite to point towards nadir as the applied gravity gradient torque does not distinguish between the antenna-end and the tip-mass end of the satellite. This means that some form of an active control system is still required to be able to point a directional antenna towards nadir. A combination of the two methods (permanent magnet and gravity gradient boom) can provide a reasonable pointing where the direction of the satellite pointing will depend on the instantaneous position of the satellite, but when it comes to placement of a directional antenna, the nature of the gravity gradient boom deployment still results in a 50% chance that the antenna may point in the opposite direction of the desired vector.

While passive magnetic pointing may not provide an accurate antenna pointing capability, its simplicity and effectiveness merit a closer investigation. In particular, the geomagnetic north pole is tilted away from the geodetic north pole in a way that the local magnetic field line in LEO may provide enough pointing torque for directional antennas to perform rough pointing. A study of the Earth's magnetic field lines in LEO near USNA reveals a possible passive-magnetic pointing solution that may enable the satellites to be able to point towards the USNA ground station without requiring any active control. The focus of this research is on investigating the feasibility of using a permanent magnet onboard a CubeSat to passively point the antenna towards the ground station in the absence of other active attitude control systems. Taking into consideration the latitude of USNA, a magnetically stabilized satellite can point close enough to nadir to keep the ground station within a typical beam width of S- and X-band patch antenna. This pointing enables low cost CubeSats to

implement higher-gain, directional antennas without implementation of a high-cost attitude control system. This paper describes the implementation method of passive-magnetic pointing on a representative 3U CubeSat, and characterizes the expected pointing accuracy, communication link performance, and ground station contact time using a typical COTS S- and X-band patch antenna.

2 Passive Magnetic Pointing Implementation

2.1 Magnetic Field Line and Nadir Pointing

As mentioned in the previous section, passive magnetic pointing is often used on less-complex CubeSats [5,7–11]. The main drawback of this method is that it cannot be used to point the satellite in a desired direction. For ground stations located in certain regions of the Earth, however, magnetic pointing may provide enough pointing capability to be used as a passive antenna pointing method. For satellites attempting to make contact with higher-latitude ground stations, passive magnetic pointing can be achieved by placing the patch antenna on the north-pole-facing surface. Permanent magnets in orbit will naturally point towards the magnetic north pole, following the local magnetic field line. As the magnetic north pole of the Earth's magnetic field does not coincide with the physical location of the North Pole on the Earth's surface, a permanent magnet in orbit will point closer to nadir direction as the satellite moves higher in latitude. The advantage of the ground stations located at higher-latitudes is that the magnetic dipole direction starts to approach nadir with increasing latitude. This alignment is depicted in Fig. 1. This orientation change for a satellite with a directional antenna mounted on the nadir-facing surface results in the target ground station to be within its beamwidth during a pass using passive magnetic stabilization method. This is depicted in Fig. 2. In this configuration, the directional antenna is centered on the long-axis of the CubeSat and is not affected by the rotation about this axis which cannot be controlled. Accordingly, no other passive or active controls are required to be able to point the directional antenna in the general direction of the ground station.

Geomagnetic latitudes and directions of the magnetic field varies depending on location (longitude/latitude), time, and altitude. In addition, the magnetic north pole is not coincident with the geographic north pole and as a result, the magnetic latitude line moves more southerly over the Americas [13,14]. This "dip" in the magnetic lines is advantageous for satellites passing over ground stations in North America because for the same geographical latitude the local magnetic latitude is higher, resulting in the local magnetic field to point more towards the nadir direction [9,15]. For this research, the analysis is performed with a set date of 19 JUN 2024

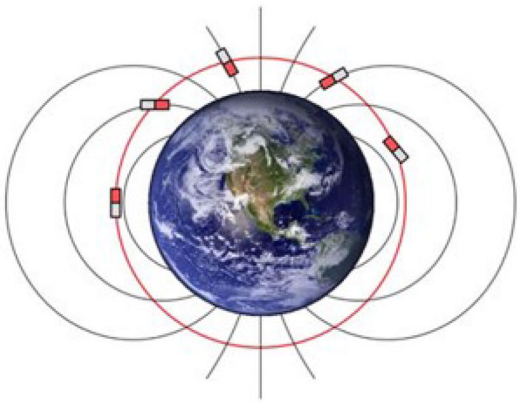

Fig. 1 Depiction of satellite magnet aligning with the local earth field direction (credit: University of Colorado, Boulder) [12]

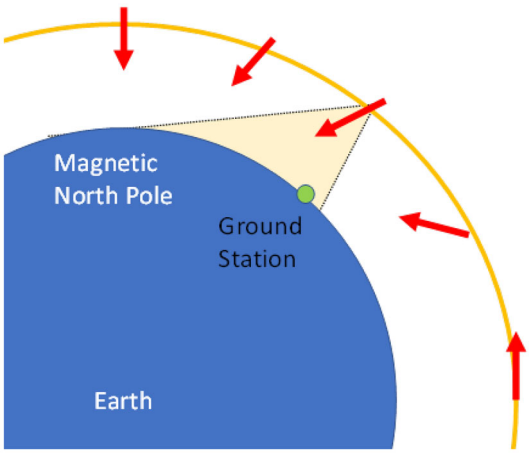

Fig. 2 The beam of magnetically-pointed antenna making contact with the ground station

to coincide with the estimated future on-orbit demonstration CubeSat launch. The main parameter used for assessing the satellite/antenna pointing performance is the off-nadir angle, defined as the angle between the local nadir vector and the local magnetic field vector pointing towards the magnetic north, as depicted in Fig. 3. In case of the ground station at USNA, the overhead satellite using a permanent magnet for antenna pointing will have 28° off-nadir angle [15]. This angle is close to the typical patch antenna half-power beamwidth, and results in closing the link without requiring an active attitude control system. Detailed analysis of this performance is described in following sections.

2.2 Satellite Setup

As the satellite moves through its orbit, the magnetic field direction relative to the satellite body will be constantly changing. Accordingly, some form of angular rate damping is required to prevent large oscillations in the pointing angle

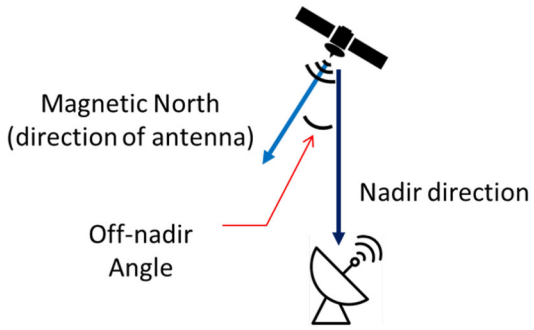

Fig. 3 Definition of off-nadir angle

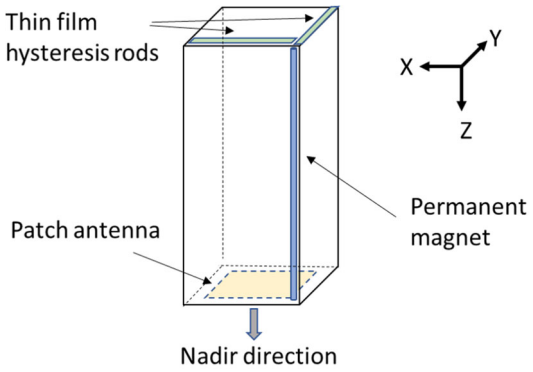

Fig. 4 Hysteresis rods and permanent magnet configuration of the 3U CubeSat

of the satellite. One simple, passive method for damping out the angular rates in LEO is use of hysteresis material [8,16]. Attaching hysteresis rods or strips will dissipate rotational energy by interacting with the changing magnetic field direction. While use of soft ferromagnetic material as hysteresis rods or thin film rods (TFR) has been widely studied and implemented, predicting their effectiveness remains complex and difficult due to their effectiveness being dependent on multiple factors such as size, shape (elongation), volume, material, manufacturing processes, arrangement, and orientation relative to other magnetic materials in proximity. A detailed modeling is therefore outside the scope of this paper and is not performed. However, a baseline design is proposed here based on the research done by Farrahi and Sanz-Andres [17] with analysis to predict the pointing performance as applied to the notional 3U CubeSat presented in this paper. Some hysteresis damping can also occur from the conductive skin of the spacecraft as it spins inside an external magnetic field [18], but this effect is much smaller than damping from hysteresis rods, and is ignored for this analysis.

In selecting shape and size of the hysteresis material, it is noted that the increase in width has an advantage in both the amount of energy dissipated and also decreasing the effect of varying magnetic field [17]. When considering circular cross-section rods (CCSR) vs. thin film rods, it is found that CCSR is more effective than TFR when rod length is increased [17]. The challenge is that, given the orientation of the satellite, the CCSR will have to be located at the ends of the CubeSat, resulting in rod lengths being limited to a maximum dimension of 10 cm. At this length, a TFR is more effective in dissipating energy [17]. TFRs can also be put on the long surface of the satellite, in perpendicular orientation, and this allows for the TFR material to be large in size, increasing their effectiveness. For the ranges of possible sizes considered for the 3U CubeSat where the length of the potential hysteresis rod cannot exceed 30 cm, TFR performs better throughout the design range [17], and accordingly, a TFR type hysteresis material was chosen for this analysis. The TFR configuration, along with the permanent magnet placement is shown in Fig. 4.

Table 1 Material selection and sizes

Item	Hysteresis rod (each)	Permanent magnet
Material	HyMu-80	Alnico-5
Coercivity (A/m)	1.59	5.09×10^4
Width (cm)	0.3	0.32
Height (cm)	0.1	0.32
Length (cm)	5.0	25.00

For maximum damping performance, the hysteresis rods must be perpendicular to the magnetic field lines when the permanent magnet is aligned with the magnetic field [9]. Also, to have damping authority in both axes, two hysteresis rods orthogonal to each other are needed, as shown in Fig. 4. One issue with this configuration is that the hysteresis rods also contribute to the system's magnetic moment, resulting in the permanent magnet's axis not being perfectly aligned with the local magnetic field line. As the rotation about this axis cannot be controlled using passive magnetic control, this pointing angle cannot be controlled, and must be accounted as a pointing error when considering the off-nadir angle performance. By increasing the magnet size to be much larger than that of the hysteresis materials, however, this stabilization error can be reduced to near-zero, making it negligible [9]. The material selection and configuration for this research (shown in Table 1) was chosen to achieve a stabilization error angle less than 0.5°, as demonstrated in the following sections. The estimated damping performance of the system is then applied in analyzing the predicted on-orbit pointing performance of the CubeSat.

2.3 Simulation Parameters

The orbit chosen for this analysis was a 400 km circular orbit with inclination of 98.7° yielding an orbital period of 92.5 min. The initial attitude was randomly assigned with initial body rates of less than a degree per second.

The attitude performance was simulated incorporating both attitude kinematics and the rigid body dynamics that result from the magnetic field interactions. This model used quaternions to describe the attitude in the form of $[q_1,\ q_2,\ q_3,\ q_4]$ with q_4 as the scalar term. The time derivative of the quaternion vector, $\boldsymbol{q} = [q_1\ q_2\ q_3]^{\mathrm{T}}$, was captured by the kinematic relationships [19]

$$\dot{\boldsymbol{q}} = \frac{1}{2}(q_4\boldsymbol{\omega} - \boldsymbol{\omega} \times \boldsymbol{q}), \tag{1}$$

$$\dot{q}_4 = -\frac{1}{2}(\boldsymbol{\omega} \cdot \boldsymbol{q}), \tag{2}$$

where $\boldsymbol{\omega}$ was the vector of spacecraft angular rates.

The spacecraft dynamics, including the gyroscopic effects were [19]

$$\dot{\boldsymbol{\omega}} = \boldsymbol{I}^{-1}(\boldsymbol{T}_{mag} + \boldsymbol{T}_{hyst} + \boldsymbol{T}_{gg} - \boldsymbol{\omega} \times \mathbf{I}\,\boldsymbol{\omega}), \tag{3}$$

where $\boldsymbol{I}$ was the Inertia matrix for the spacecraft, $\boldsymbol{T}_{mag}$ was the torque due to the magnet field interaction, $\boldsymbol{T}_{hyst}$ was the torque due to hysteresis rods, and $\boldsymbol{T}_{gg}$ was the disturbance due to gravity gradient torques and was defined by [20]

$$\boldsymbol{T}_{gg} = \frac{3\mu}{\|\boldsymbol{R}\|^3}(\hat{\boldsymbol{R}}_b \times I\ \hat{\boldsymbol{R}}_b), \tag{4}$$

with μ as the Earth's gravitational constant, $\|\boldsymbol{R}\|$ as the vector norm of the orbital radius vector, and $\hat{\boldsymbol{R}}_b$ which was the direction of the radius of the spacecraft orbit represented in the spacecraft body frame.

The magnetic field torques were defined by [20]

$$\boldsymbol{T}_{mag} = \mathbf{m} \times \mathbf{B_b}, \tag{5}$$

where $\mathbf{m}$ was the magnetic dipole moment for the entire spacecraft including the permanent magnet fixed at 2.57 A m^2 along the Z body axis and $\mathbf{B_b}$ was the magnetic field of the earth in the spacecraft body frame. The hysteresis rods are very complicated to properly simulate and thus were assumed to be a linear function of the spacecraft angular rates, using a typical value used for CubeSats from the past studies and missions [8–11].

The permanent magnet should be sized such that the magnetic field torques are larger than the disturbance toques. Using (4), the gravity gradient disturbance torques for a 3U CubeSat at 400 km orbit are on the order of 10^{-8} N m. The magnet described above yields magnetic torques on the order of 10^{-7} N m (see Fig. 5).

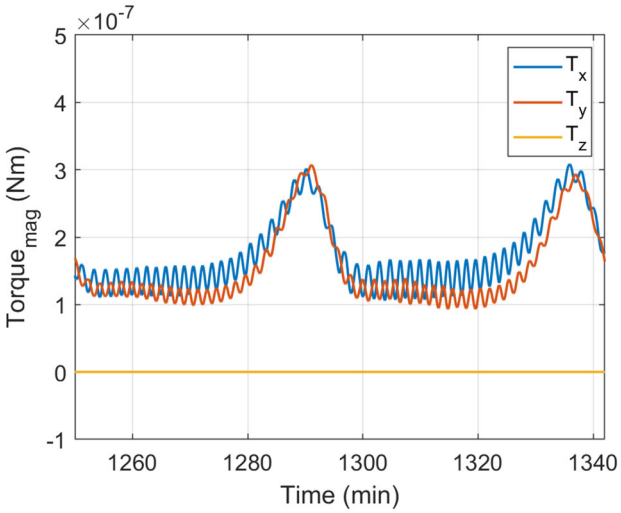

Fig. 5 Magnetic field torques over a single orbit in steady state

If the magnet is properly sized, when combined with the hysteresis rods, the spacecraft attitude remains relatively stable, though always in motion seeking to align itself with the Earth's magnetic field lines. After the initial alignment period, the body rates were maintained within ±0.06°/s of the required 0.13°/s, which included accounting for gravity gradient disturbances.

3 Attitude Control Performance

3.1 Detumbling Performance

Magnets are very effective at passively detumbling a spacecraft after launch. Normally, the magnetic dipole moment of the spacecraft is controlled using current to achieve the desired torques, but in the case of a permanent magnet, this magnetic torque will be present any time the magnetic field of the spacecraft and the earth are not aligned. Based on the satellite setup scenario described in previous sections, detumbling performance of the 3U CubeSat was characterized including expected disturbance torques. The body axes are shown in Fig. 4, where the z-axis aligns with the long-axis of the 3U CubeSat, and points towards nadir. For this analysis, the initial tumbling rate was set to 5°/s. As shown in Figs. 6 and 7, the proposed magnetic attitude stabilization setup is able to detumble the satellite in approximately 40 min. The corresponding magnetic torques produced by the permanent magnet and also the induced hysteresis torques from the TFRs are shown in Figs. 8 and 9.

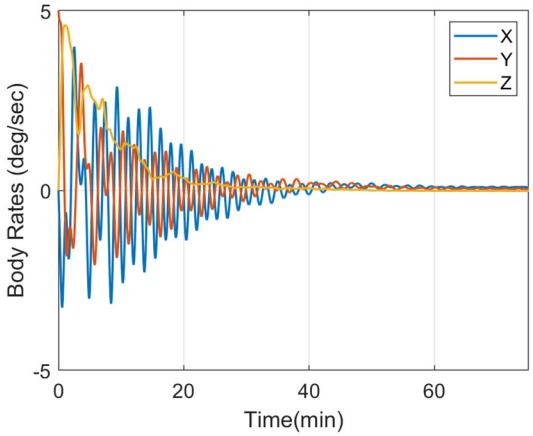

Fig. 6 Initial de-tumbling performance when starting at 5°/s

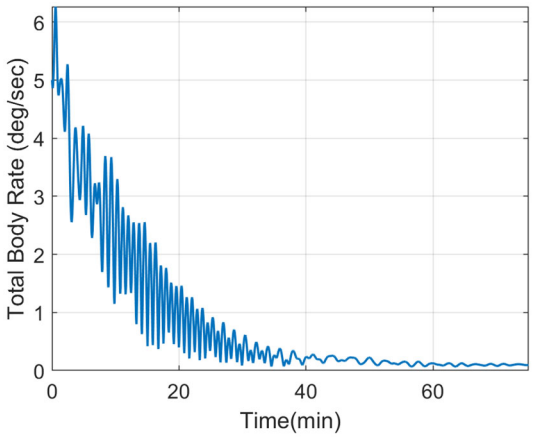

Fig. 7 Rate magnitude during de-tumbling when starting at 5°/s

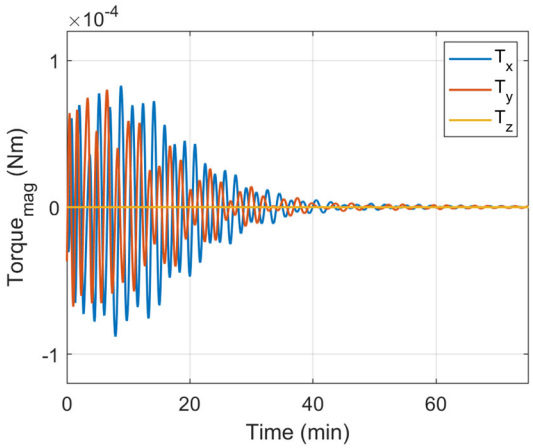

Fig. 8 Magnetic torques during de-tumbling when starting at 5°/s

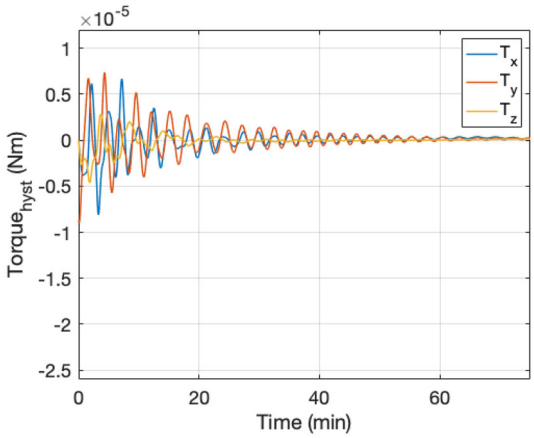

Fig. 9 Hysteresis torques during de-tumbling when starting at 5°/s

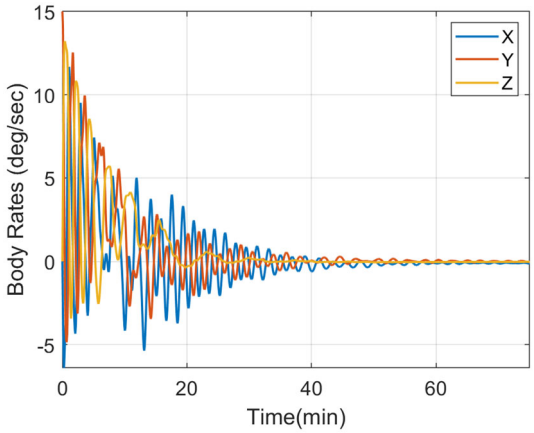

Fig. 10 Initial de-tumbling performance when starting at 15°/s

A similar analysis was performed for a higher initial tumbling rate of 15°/s (Fig. 10). The resulting plots are shown in Figs. 11, 12 and 13. As can be seen in the figures, detumbling is still achieved in approximately 40 min. As the body rates increase, the torque output from the magnetic system is also increased. The analyses show that the permanent magnets and hysteresis TFRs are sufficiently oversized to overcome the initial satellite tumble and stabilize it down to a reasonable body rates.

3.2 Pointing Accuracy

In addition to the pointing stability, another important performance parameter is pointing accuracy. As the satellite progresses throughout its orbit, the local magnetic field is constantly changing, resulting in the satellite pointing direction also changing as the magnetic dipole tracks the local magnetic field lines. The polar orbit assumed in this analysis presents the worst case scenario for magnetically

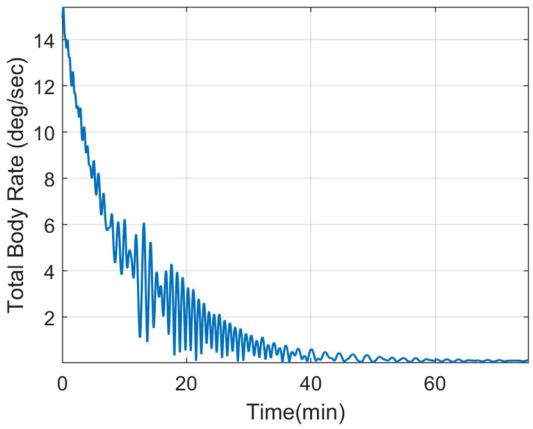

Fig. 11 Magnitude of rate during de-tumbling performance when starting at 15°/s, just with different scaling

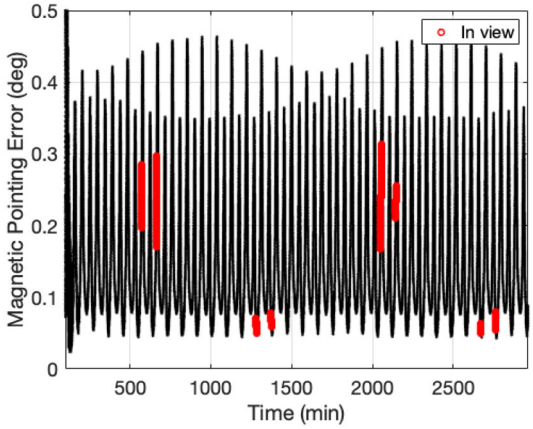

Fig. 14 *Z*-axis pointing error with respect to magnetic field line

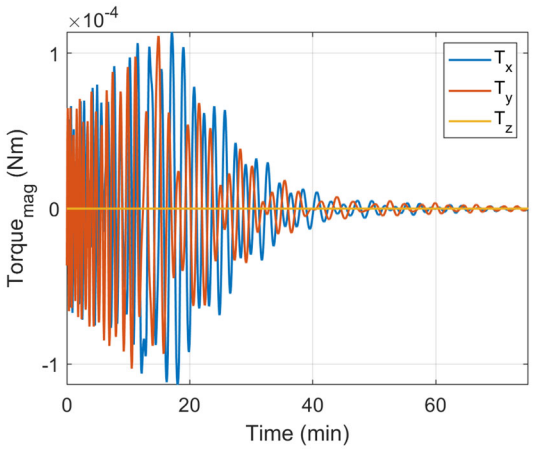

Fig. 12 Magnetic torques during de-tumbling when starting at 15°/s

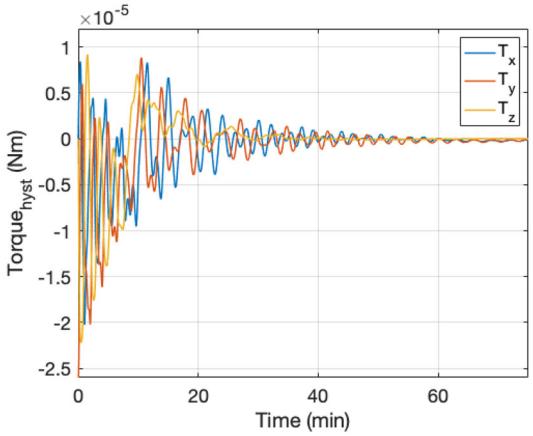

Fig. 13 Hysteresis torques during de-tumbling when starting at 15°/s

pointed satellite because satellites passing over the magnetic poles will go through rapid angular changes. Assuming the satellite configuration previously described, an analysis was performed to quantify the pointing error of the satellite's magnetic dipole axis (body *Z* axis) to the local magnetic field line. Figure 14 shows the pointing error over 2 days. Marked in red are time durations when the satellite is in view of USNA ground station, at approximately 38° latitude. As can be seen, the pointing error is well within 1° of the local magnetic field line as the sizing of the permanent magnet for this proposed configuration easily over-powers disturbance torques and keeps it aligned with the local, changing magnetic field. This also means that the off-nadir angle, as defined in Fig. 3, can be determined using the local magnetic field direction to within 1° accuracy. In case of USNA ground station at approximately 38°N latitude, an off-nadir angle of 28° can be achieved [15].

3.3 Ground Contact Analysis

Orbital dynamics dictates that every orbit will not produce a pass or access between the satellite and the ground station. Typically for a low earth orbit, the expectation is not more than six and realistically three to five good passes per day, though this is dependent on the orbit inclination and the latitude of the ground station. Figure 15 show the expected passes for a polar or sun-synchronous orbit over 2 days. The typical two to three passes for each of the ascending and descending period are clearly visible. Over these 2 days, the first two passes were descending followed by three ascending, then three descending and finally two ascending passes. A 3U CubeSat configured to the proposed setup will pass over USNA ground station with an off-nadir angle of 28° [15]. In this analysis, the satellite is assumed to have a S- or X-band patch antenna with a beamwidth of 120°. Assuming this ±60° boresight, Fig. 15 shows both the times when the satellite is over the horizon (marked "Above Horizon") as viewed from USNA ground station, as well as when the ground station is actually within the satellite antenna's beamwidth (marked "In view").

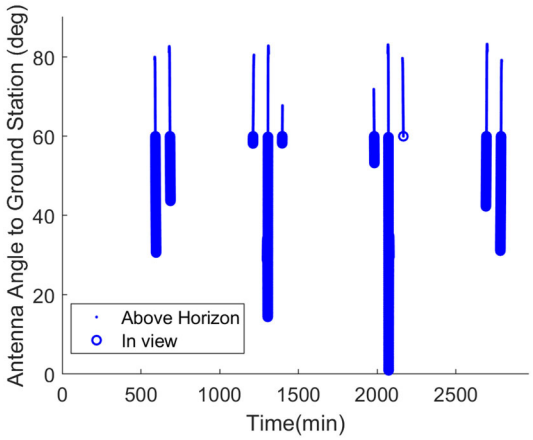

Fig. 15 Boresight error angles over two full days

Table 2 Times for possible ground station contacts over 2 days

Pass number	Over horizon (s)	In view (s)	Percent of pass (%)
1	533.0	280.0	50.6
2	534.0	184.5	34.6
3	381.5	20.5	5.4
4	602.0	346.5	57.6
5	121.5	19.0	15.6
6	238.5	70.5	29.6
7	603.5	347.0	57.5
8	341.5	0.0	0.0
9	549.5	207.0	37.7
10	537.0	267.0	49.7

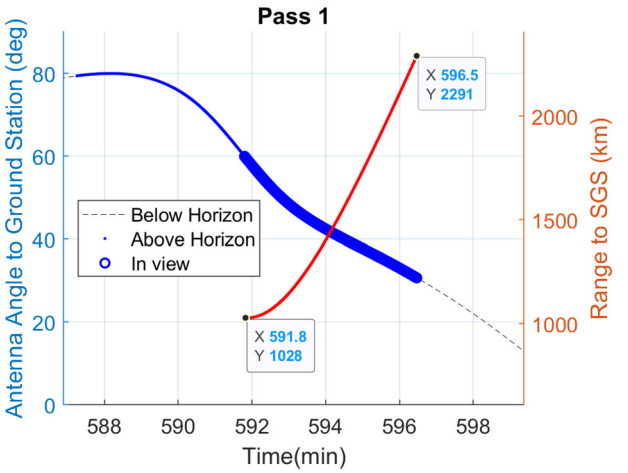

Fig. 16 Example of average-duration pass with close approach to the ground station

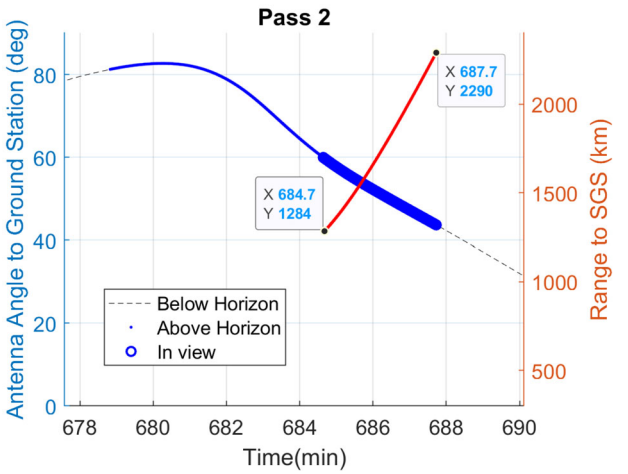

Fig. 17 Example of average-duration pass without close approach to the ground station

Each pass resulted in differing contact durations based on the location of the spacecraft with respect to the ground station. Table 2 shows the times for each pass in Fig. 15 and the percent of time the ground station spent in the beamwidth of the satellite antenna. The passes from the first day (passes 1–5) accumulated 850.5 s of possible satellite communication contact time which represented 38.8% of the total possible above-the-horizon time. For day 2 (passes 6–10), there was 891.5 s of contact time representing 39.3% of the available time.

The progression of the boresight with respect to the ground station are shown in Figs. 16, 17, 18 and 19. In a descending pass, the satellite comes over the threshold of 5° above the horizon (shown as dots or an unbroken line) but is not pointing in the correct direction. As its orbital motion progresses toward the equator, the ground station enters the 60° beamwidth of the boresight (shown as thick lines or circles) and stays within view until the spacecraft passes below the horizon southbound. Additionally, the range from the spacecraft to the ground station is presented in Figs. 16, 17, 18 and 19 as a red line, with the endpoint values annotated. This progression is demonstrated in Figs. 16 and 17 which are close up view of the first two descending passes, also the first two passes in Fig. 15.

As expected, an ascending pass almost mirrors the progression of a descending pass. Here, the satellite comes over the horizon with the ground station already in the beamwidth. The pass progresses as the ground station exits the beamwidth and the satellite continues until it goes below the ground station horizon. This progression is demonstrated in Fig. 18 which is a close up view of the second descending pass, or the fourth pass in Fig. 15.

The beneficial dip in boresight error is not unique to ascending passes. It occurs any time the satellite boresight sweeps across the ground station because of the east-west orbital motion of the ground track. Figure 19 shows similar behavior, except in this case, the boresight actually passes

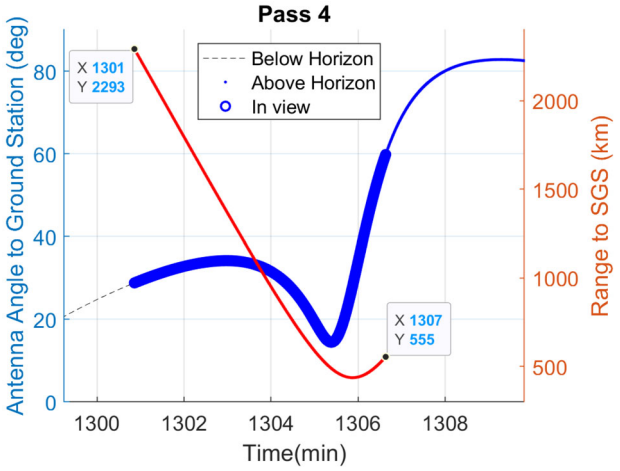

Fig. 18 Example of long-duration, overhead north-to-south pass

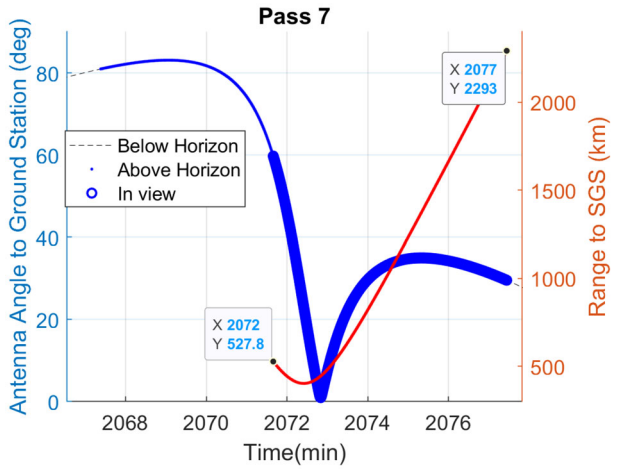

Fig. 19 Example of long-duration, overhead south-to-north pass

directly over the ground station causing the boresight error to go to zero.

4 Communication Link Performance

4.1 Power Generation Prediction

Using hysteresis rods to passively assist with the pointing of a high bandwidth S-band antenna accomplishes only part of the solution. A key part to any communication system of a spacecraft is the power necessary to transmit the required signal. The spacecraft must generate sufficient power to operate the radio and close the link with the ground station. Based on per orbit operations in the proposed orbital regime, a power analysis was performed to show the overall effectiveness as a potential solution to the higher data needs of a magnetically pointed CubeSat.

A baseline power generation performance analysis was first performed. Based on past and expected future uses, a high efficiency, multi junction solar cell was used in this analysis. Seven 26.6 cm^2 Ultra Triple Junction (UTJ) cells with an efficiency of 28% were mounted on each long side of the 3U CubeSat design for the initial simulations. The top face also included two solar cells, but the bottom face included only the communications patch antenna. Additionally, a lifetime degradation of 2.75% [21] and a conservative power efficiency transmission of 80% to the load further degraded the system performance.

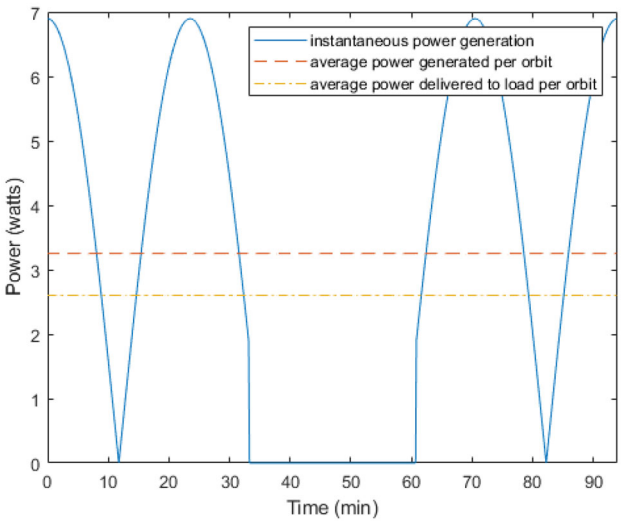

Fig. 20 Updated power generation per orbit with both averages.png

Solar cell attitude relative to the sun was incorporated into the simulation for all cells, as were eclipse times, but any benefit from Earth albedo was omitted. As can be observed in Fig. 2, the orientation of the CubeSat will change 180° from the equator to the poles. The passive attitude control will naturally orient the small side toward the Earth so that the long sides would remain pointed towards the Sun for a larger portion of time. Thus, only the long side were simulated with solar cells. Another conservative assumption was that only one long side was facing the sun at a time. The power consumption for other subsystems was estimated at 2.5 W total when not transmitting. Based on the above conservative assumptions, an initial simulation was done in MATLAB using [21]

$$P_{\text{gen}} = P_{\text{sun}} \times A \times L_d \times \cos\theta. \tag{6}$$

Here, P_{gen} is the power generated by the solar panel, P_{sun} is the solar flux, A is the solar panel (covered by cells) area, L_d is the lifetime degradation of the solar cells, and θ is the incident sun angle. Figure 20 shows the instantaneous power generated, the average power generated per orbit, and the average power delivered to the load per orbit. With an average solar flux of 1360 W/m^2, the average power generation to the load per orbit is 2.6 W. The results show that sufficient

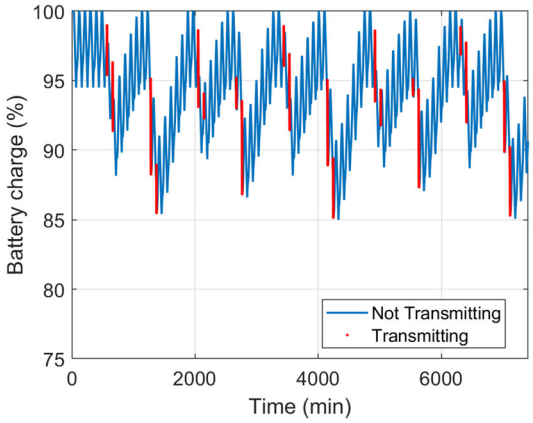

Fig. 21 Battery charge state over 5 days

power can be generated per orbit to operate the CubeSat, keeping in mind that this power is using the most conservative assumptions.

Since this initial simulation was only conducted for one orbit and did not take into account the communication subsystem, a more detailed analysis was conducted using the actual sun angles and incorporating periodic communication transmissions when over the ground station. Figure 21 shows the state of battery charge over five full days of simulation. It can be clearly seen that sufficient power is generated to fully charge the batteries. The assumption was made that the full 20 W were needed continuously during transmission (red data points) and 2.6 W continuous power when not transmitting (blue data points). The results of this analysis showed that 2.6 W can be delivered to the satellite bus with the maximum depth of discharge of 15% over a 5 day simulation, including the high power draw of the communication subsystem. The results demonstrate that a 3U CubeSat with a simpler body-mounted solar panel configuration is sufficient to provide 20 W of power for transmission using the proposed configuration, made possible by reducing the potential additional power consumption from an attitude control device.

5 Data Throughput Analysis

To characterize the overall resulting communication link performance of the proposed attitude control scheme, a link analysis was performed for a satellite in 400 km altitude circular orbit. Two cases were evaluated. A more conservative case was based on a probability of bit error of 10^{-6}, desired link margin of at least 3 dB, and nominal S- and X-band antenna gains derived from their beamwidths. The more aggressive configuration used a probability of bit error of 10^{-5} and antenna gains pulled from datasheets of commercially-available Haigh-Farr S- and X-band patch antennas.

Table 3 provides the conservative and aggressive link estimates for the S- and X-band communications system performance. For all cases, a conservative estimate of 2 W of total transmit power, or 10% Tx power efficiency from the available 20 W power for transmission was assumed. From the analysis described previously, a total contact time of 850 s/day was used. QPSK modulation was selected as a reasonable trade-off between bandwidth, complexity, and performance. The link was evaluated for a 5° minimum elevation angle. In Table 3, the cable and connector losses at the transmitter were captured as TX Losses. RX Losses capture

Table 3 Link analysis for S- and X-band CubeSat at 400 km altitude

	S-Band (2.25 GHz)		X-Band (8.25 GHz)	
	Cons.	Aggr.	Cons.	Aggr.
TX power (dBm)	33	33	33	33
TX losses (dB)	0.5	0.5	0.5	0.5
RX losses (dB)	4.5	4.5	4.5	4.5
TX antenna gain (dBi)	2.0	5.0	2.0	7.0
Path loss (dB)	164.6	164.6	175.9	175.9
RX antenna gain	37.1	37.1	48.3	48.3
Total received power (dBm)	−141.4	−134.8	−149.4	−141.7
Bit error rate	10^{-6}	10^{-5}	10^{-6}	10^{-5}
Minimum $\frac{E_b}{N_0}$ (dB)	10.5	9.6	10.5	9.6
Desired $\frac{E_b}{N_0}$ (dB)	13.5	12.7	13.5	12.7
Maximum noise power (dBm)	−122.1	−114.4	−129.9	−122.1
Max bandwidth for $\frac{E_b}{N_0}$ (kHz)	90.0	350	15.0	72.0
Max data rate (QPSK) (kbps)	90.0	350	15.0	72.0
Total data for 850s (MB)	9.1	35.5	1.5	7.3

the cable, connector, and polarization losses at the receiver. The ground station parameters are based on the current capabilities of the USNA satellite ground station. The station has a +37 dBi gain at S-Band and +48 dBi gain at X-Band and operates with a 60% aperture efficiency. The assumed generic system noise temperature is 750 K. (In comparison, a commercial or research-grade ground station would have a noise temperature in the 350–500 K range, resulting in a 6–10 dB improvement in link margin and higher achievable data rate that what the analysis result shows.)

The results from the link budget shows that a maximum data rate of 350 kbps at S-Band and 72 kbps at X-Band can be achieved, resulting in a total payload transfer of 35.5 MBytes and 7.3 MBytes/day, respectively. The more conservative analysis suggests data rates of 90 kbps and 15 kbps, with total payload transferred of 9.1 and 1.5 MBytes/day. It should be noted that these are conservative estimates based on the worst-case position of the CubeSat at the horizon. For the same 3 dB link margin, the data rates double when the CubeSat is at 10° elevation angle, then double again at 20° elevation. These potential higher data rates were not factored in for this analysis. Also, using a modulation scheme that could adapt to changing link conditions would clearly result in a higher total data transfer.

This result can be compared to a typical university CubeSats that use 9600 bps communication. Assuming an omni-directional antenna, the available contact time for these satellites for the same analysis increases to approximately 2200 s/day. This means that there is a potential for 2.6 MB of data to be downlinked in a day, assuming 0°, immediate contact at horizon. It can therefore be seen that omnidirectional data throughput is generally lower than what S- and X-band communication with a simple magnetic pointing system can deliver.

6 Conclusions

Lower data rate communications using VHF and UHF are popular in CubeSat projects. The ability to implement an omni-directional antenna setup means that the satellite will not require a attitude control system for communication purposes, drastically reducing the system resource demand and cost of the project. However, as more CubeSat projects are pushed towards higher frequency bands, implementation of an attitude control system becomes a big burden on lower budget student projects.

A method for utilizing a simple magnetic pointing to point the antenna is proposed in this study. Taking into account the current and near future geomagnetic field lines, CubeSats making contact with the ground stations in North America can utilize a simple, permanent-magnet for near-nadir pointing to accomplish directional communication with the ground station. LEO satellites with a magnet aligned with its antenna will be able to point towards nadir within approximately 35° or less, placing the target ground station within its typical beamwidth for about 1/3 of the total available contact time. For a 400 km polar orbit, approximately 10 to 35 MB for S-band or 1 to 7 MB for X-band can be downlinked in a day. This can be accomplished without additional attitude control devices. Power analysis also shows that, due to the absence of attitude control system, and typical 3U CubeSat is able to provide enough power without any deployable solar panels, further reducing the project cost and complexity. As the geomagnetic field continues to shift, the downlink performance will also vary in the future, but for the next few years, CubeSats with ground stations in North American may be able to implement S- or X-band communication without an active attitude control system, simply by utilizing passive magnetic pointing.

Declarations

Conflict of interest On behalf of all authors, the corresponding author states that there is no conflict of interest.

References

1. Poghosyan A, Golkar A (2017) CubeSat evolution: analyzing CubeSat capabilities for conducting science missions. Prog Aerosp Sci 88:59–83. https://doi.org/10.1016/j.paerosci.2016.11.002
2. Saeed N, Elzanaty A, Almorad H, Dahrouj H, Al-Naffouri TY, Alouini M-S (2020) CubeSat communications: recent advances and future challenges. CubeSat Communications IEEE Commun Surv Tutorials 22:1839–1862. https://doi.org/10.1109/COMST.2020.2990499
3. Selva D, Krejci D (2012) A survey and assessment of the capabilities of Cubesats for Earth observation. Acta Astronautica 74:50–68. https://doi.org/10.1016/j.actaastro.2011.12.014. Accessed 03 June 2020
4. Gerhardt DT, Palo SE (2016) Volume magnetization for system-level testing of magnetic materials within small satellites. Acta Astronautica 127:1–12. https://doi.org/10.1016/j.actaastro.2016.05.017
5. Rawashdeh, S.A.: Passive attitude stabilization for small satellites. Master's thesis, University of Kentucky (2010)
6. Rawashdeh SA (2019) Attitude analysis of small satellites using model-based simulation. Int J Aerosp Eng 2019:1–11. https://doi.org/10.1155/2019/3020581. Accessed 03 June 2020
7. Santoni F, Zelli M (2009) Passive magnetic attitude stabilization of the UNISAT-4 microsatellite. Acta Astronautica 65(5–6):792–803. https://doi.org/10.1016/j.actaastro.2009.03.012. Accessed 03 June 2020
8. Ivanov DS, Ovchinnikov MY, Pen'kov VI (2013) Laboratory study of magnetic properties of hysteresis rods for attitude control systems of minisatellites. J Comput Syst Sci Int 52(1):145–164. https://doi.org/10.1134/S1064230712060032. Accessed 02 June 2020
9. Levesque J-F (2003) Passive magnetic attitude stabilization using hysteresis materials. Technical Report SIgMA-PU-006-UdeS, Université de Sherbrooke, Sherbrooke, Quebec, Canada. http://

courses.engr.uky.edu/ideawiki/data/media/projects/active/kysat/workspace/sigma_pu_006_udes.pdf. Accessed 18 Mar 2021
10. Fiorillo F, Santoni F, Ferrara E, Battagliere ML, Bottauscio O, Graziani F (2010) Soft magnets for passive attitude stabilization of small satellites. IEEE Trans Magn 46(2):670–673. https://doi.org/10.1109/TMAG.2009.2033345. Accessed 02 June 2020
11. Gerhardt DT (2014) Small satellite passive magnetic attitude control. PhD dissertation, University of Colorado Boulder, Boulder, CO. https://scholar.colorado.edu/concern/graduate_thesis_or_dissertations/s1784k881. Accessed 18 Mar 2021
12. Colorado Student Space Weather Experiment ≫ Attitude determination and control subsystem. https://lasp.colorado.edu/home/csswe/system/subsystems/adcs/. Accessed 03 Oct 2020
13. SPACE WEATHER: maps of geomagnetic latitude. https://spawx.nwra.com/spawx/maps/maplats.html. 16 June Accessed 2020
14. Ovchinnikov MY, Penkov VI, Roldugin DS, Pichuzhkina AV (2018) Geomagnetic field models for satellite angular motion studies. Acta Astronautica 144:171–180. https://doi.org/10.1016/j.actaastro.2017.12.026
15. Kang JS, King JT, Anderson CR, Sanders MH (2020) Passively pointing directional satellite antenna by leveraging Earth's magnetic field. IEEE Commun Surv Tutor **22**(3):50–68. https://doi.org/10.1109/COMST.2020.2990499. Conference Name: IEEE Aerospace Conference
16. Ovchinnikov M (2012) Attitude dynamics of a small-sized satellite equipped with hysteresis damper. Adv Astronaut Sci 145:311–330
17. Farrahi A, Sanz-Andres A (2013) Efficiency of hysteresis rods in small spacecraft attitude stabilization. Sci World J 2013:1–17. https://doi.org/10.1155/2013/459573. Accessed 02 June 2020
18. Surkov VV (2020) Effect of geomagnetic field on motion of passive conductive satellites. Geomagn Aeron 60(2):192–204. https://doi.org/10.1134/S0016793220020152
19. Wie B (2008) Space vehicle dynamics and control. AIAA, Reston
20. Sidi MJ (2000) Spacecraft dynamics and control: a practical engineering approach. Cambridge University Press, New York
21. Space Mission Engineering: the New SMAD. Space Technology Library, vol 28. Microcosm Press, Hawthorne (2011)